

Encapsulation of AgNPs within Zwitterionic Hydrogels for Highly Efficient and Antifouling Catalysis in Biological Environments

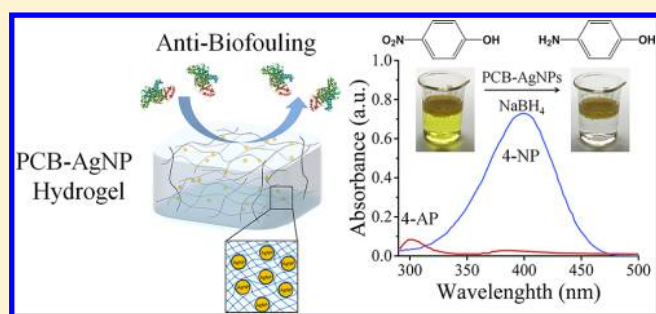
Jiayin Song,[†] Yingnan Zhu,[†] Jiamin Zhang, Jing Yang, Yan Du, Weiwei Zheng, Chiyu Wen, Yumiao Zhang, and Lei Zhang*[✉]

Department of Biochemical Engineering, School of Chemical Engineering and Technology, Frontier Science Center for Synthetic Biology and Key Laboratory of Systems Bioengineering (MOE), and Collaborative Innovation Center of Chemical Science and Engineering (Tianjin), Tianjin University, Tianjin 300072, PR China

Qingdao Institute for Marine Technology of Tianjin University, Qingdao 266235, PR China

S Supporting Information

ABSTRACT: Silver nanoparticles (AgNPs) have been widely used as catalysts in a variety of chemical reactions owing to their unique surface and electronic properties, but their practical applications have been hindered by severe aggregation. The immobilization of AgNPs is crucial to preventing their aggregation or precipitation as well as to improving their reusability. Herein, we developed a facile route for the reductant-free in situ synthesis of AgNPs in zwitterionic hydrogels. Via this method, the embedded AgNPs had a uniform distribution, high activity, and antibiofouling capability. The catalytic reduction of 4-nitrophenol (4-NP) to 4-aminophenol (4-AP) using polycarboxybetaine-AgNPs (PCB-AgNPs) could achieve >95% conversion efficiency within 5 min. Meanwhile, the normalized rate constant k_{nor} ($10.617 \text{ s}^{-1}\text{mmol}^{-1}$) was higher than that of most of the reported immobilized nanocatalysts. More importantly, in a biofouling environment, PCB-AgNPs could still exhibit >97% initial catalytic activity while AgNPs in the PSB or PHEMA hydrogel lost ~60% activity. This strategy holds great potential for the immobilization of nanoparticle catalysts, especially for applications in biological environments.



INTRODUCTION

Silver nanoparticles (AgNPs) have received an extensive amount of attention as a result of their unique electronic and catalytic properties.¹ They can catalyze a variety of chemical reactions,^{2,3} such as the reduction of nitrophenols^{4,5} and the oxidation of methanol and ethylene.² However, similar to most metal nanoparticles, the aggregation of AgNPs is a serious problem that can undermine the surface-to-volume ratio and ultimately compromise the catalytic performance.⁶ Polyelectrolytes, inorganic ions, or biomacromolecules in ambient environments can easily induce the aggregation. For instance, the wastewater discharged from the leather industry contains a large amount of proteins⁷ that can adhere to the nanoparticles and subsequently invalidate their active sites. With the increasing demand of heterogeneous catalysis in complex environments, the facile synthesis of AgNPs catalysts with antifouling and reusable properties is of great necessity. To solve this problem, various supporting materials have been developed to protect AgNPs, such as polymer vesicles,⁸ dendrimers,⁹ carbon nanotubes,⁴ silicates,¹⁰ and hydrogels.¹¹ However, several important properties including stability, mass transfer efficiency, reusability, and fouling resistance ability are still greatly needed for an ideal supporting material.

Hydrogels are cross-linked polymeric 3D hydrophilic networks that are capable of entrapping a large amount of

water. These appealing properties render them promising candidates for AgNP immobilization.¹² Recently, zwitterionic materials have been found to be especially interesting and have attracted increasing amounts of attention because of their excellent antifouling ability.^{13,14} Zwitterionic moieties can strongly bind water molecules via the ionic solvation effect, producing repulsive forces to effectively eliminate the adsorption of proteins¹⁵ as well as the adhesion of bacteria or cells.¹⁶ In 2008, Jiang et al. reported that zwitterionic polymers, especially polycarboxybetaine (PCB), exhibited strong resistance to nonspecific protein adsorption in 100% human serum and plasma.¹⁵ In 2017, Zhang et al. showed that a PCB hydrogel coating could improve the hemocompatibility of activated carbon powder without sacrificing its adsorption performance in 100% fetal bovine serum (FBS).¹⁷ Similar to physiological environments, there are multifarious biomolecules in industrial and agricultural wastewaters.^{18–20} Without protective materials, proteins and other biomolecules are

Special Issue: Zwitterionic Interfaces: Concepts and Emerging Applications

Received: August 28, 2018

Revised: November 15, 2018

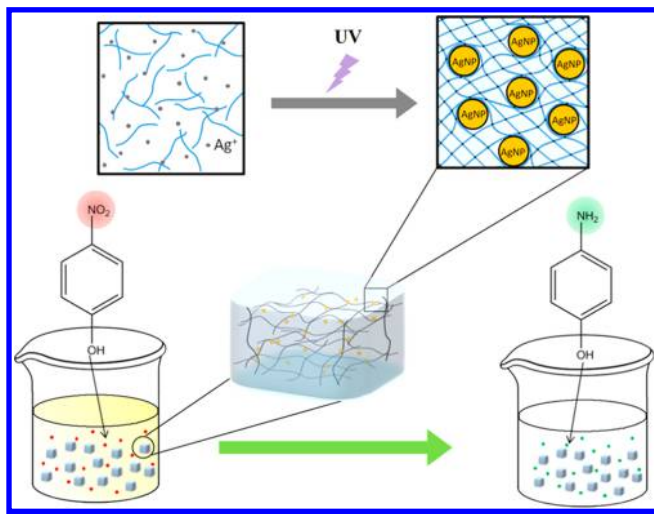
Published: December 18, 2018

inevitably prone to adsorb to metal nanoparticles by electrostatic interactions and consequently compromise their catalytic efficiency. An ideal supporting material is expected to prevent the nanoparticles from aggregation, contamination, and inactivation. Because of the hydrophilic and antifouling properties, we propose that zwitterionic hydrogels can be used as ideal matrixes for nanocatalysts immobilization, especially in biological environments.

4-Nitrophenol (4-NP) is a refractory nitroaromatic due to its high toxicity, good chemical stability,²¹ and difficult removal by natural degradation.²² It has been classified as the priority pollutant by the U.S. Environmental Protection Agency (EPA) among the top 114 organic pollutants.²³ In recent years, many methods have been developed for the oxidation or reduction of 4-NP, such as photocatalytic degradation,²⁴ the electrofenton method,²⁵ electrochemical treatment,²⁶ and catalytic reduction.²⁷ Among these methods, the reduction of 4-NP to 4-aminophenol (4-AP) with sodium borohydride has been considered to be the most efficient and green method. 4-AP is an important intermediate in synthesizing analgesic and antipyretic drugs, corrosion inhibitors, and photographic developers.^{4,8,28} However, this relatively simple and clean reaction proceeds slowly without a suitable catalyst.^{29–31} AgNPs have been reported to be an efficient catalyst in assisting borohydride for the conversion of 4-NP to 4-AP upon their unique electronic properties.^{9,32,33} It is highly desired to develop novel catalysts with well-dispersed AgNPs and stable catalytic performance to treat 4-NP before being discharged into the ambient environment.

In this work, we developed a facile method to synthesize and encapsulate AgNPs in situ in zwitterionic hydrogels for the reduction of hazardous 4-NP to eco-friendly 4-AP (Scheme 1).

Scheme 1. Catalytic Reduction of 4-NP to 4-AP by AgNP-Embedded Zwitterionic Hydrogels



Via the photopolymerization procedure,¹⁶ AgNPs and a hydrogel were formed synchronously while AgNPs were uniformly distributed in the hydrogel without any aggregation. Notably, AgNP-embedded zwitterionic hydrogels, especially PCB-AgNPs, showed superior catalytic activity compared to most of the reported immobilized AgNPs catalysts. PCB-AgNPs could also effectively maintain the catalytic activity in complex environments. Furthermore, after the catalytic

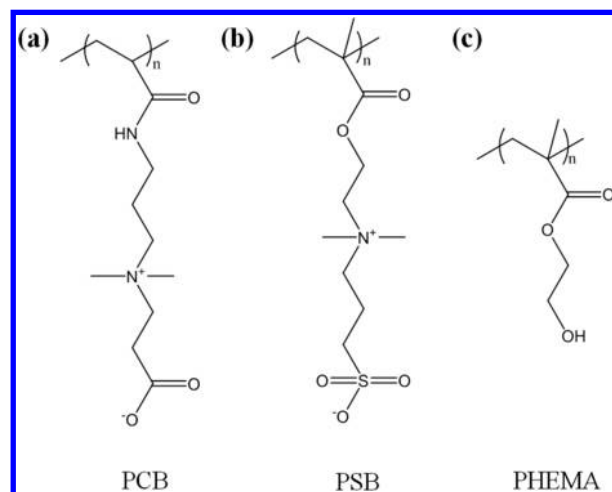
reaction, PCB-AgNPs could be easily separated and reused in cyclic catalysis.

EXPERIMENTAL SECTION

Materials. Silver nitrate (AgNO_3), sodium borohydride (NaBH_4), ethanol, and ethylene glycol were purchased from Yuanli, Tianjin. 4-NP was supplied by Aladdin. Bovine serum albumin (BSA) and FITC-BSA were purchased from Solarbio. 2-Hydroxyethyl methacrylate (HEMA) was purchased from Acros Organics, and triethylene glycol dimethacrylate (TEGDMA) and 2-hydroxy-2-methylpropiophenone (HMPF) were obtained from Adamas. *N,N*-Methylenebisacrylamide (MBAA) and *N*-(3-sulfopropyl)-*N*-(methacryloyloxyethyl)-*N,N*-dimethylammoniumbetaine (SBMA) were both purchased from TCI, Shanghai. Carboxybetaine acrylamide (CBAA) was prepared as reported previously.³⁴ All of the reagents mentioned above were used as received without purification, and the water that was used was purified to $18.2 \text{ m}\Omega$ with a Millipore Simplicity water purification system in all experiments.

Preparation of the AgNP-Embedded Zwitterionic Hydrogels. The monomer solutions of PCB (Scheme 2a) hydrogels were

Scheme 2. Chemical Structures of (a) PCB, (b) PSB, and (c) PHEMA



prepared in 1 M NaCl at a total concentration of monomer (CBAA) and cross-linker (MBAA) of 40% (w/v), and the concentration of AgNO_3 varied from 0 to 20 mM. The cross-linker (MBAA) was added to the reactant solution in a quantity of 2% (molar percent of monomer). The monomer and cross-linker were dispersed by sonication in an ice bath for 30 min. After the ultrasonic dispersion, $4 \mu\text{L}$ of HMPF was added, and the solution was mixed by gentle shaking. Then, the solutions were transferred to the space between two glass plates, separated with a 0.5 mm poly(tetrafluoroethylene) (PTFE) spacer. The photopolymerization reaction was carried out at room temperature under 365 nm UV light to polymerize the hydrogels. Each side was exposed to UV light for 10 min. After the polymerization, hydrogels were removed from the slides and cut into 0.5 mm^3 particles. The hydrogel particles were immersed in phosphate-buffered saline (PBS) for 5 days to allow water equilibration. The buffer was changed daily to remove unreacted chemicals and excess salt. The PSB (Scheme 2b) hydrogels were polymerized in a manner similar to that described above.

PHEMA (Scheme 2c) hydrogels were prepared by mixing 0.78 mL of HEMA monomer in 1.5 mL of a mixed solvent which contained 1 part ethanol, 1.5 parts ethylene glycol, and 1.5 parts AgNO_3 solution. After the addition of $30 \mu\text{L}$ of cross-linker (TEGDMA), the mixture was mixed by ultrasonic dispersion. Then, $20 \mu\text{L}$ of photoinitiator (HMPF) was added to the mixture solution. After gentle shaking, the PHEMA hydrogels were polymerized as described above.

Water Content. Before the evaluation of water content, hydrogels were fully equilibrated in PBS buffer for 5 days. Then samples were cut into $\sim 0.5 \text{ mm}^3$ particles. The wet weight of the hydrogel samples was measured after removing excess water. The dry weight was recorded after drying under vacuum at $60 \text{ }^\circ\text{C}$ for 3 days. The equilibrium water content (EWC) of the hydrogel was calculated by

$$(\text{EWC})\% = (W_w - W_d)/W_w \times 100\% \quad (1)$$

where W_w is the weight of the wet hydrogel and W_d is the weight of the dry hydrogel.

Mechanical Property and Mesh Size. The mechanical property of the hydrogels was investigated by stress–strain measurements under a standard condition. The samples were punched to be 5 mm in diameter from the as-prepared hydrogels. The compression tests were performed according to the previous work.³⁵ In brief, the hydrogel samples were compressed to fracture between the lower and upper plates at a rate of 0.2 mm/s using a mechanical tester, and the compressive modulus was determined by calculating the slope of the linear region of the stress–strain curves (typically between 10 and 15% strain). The break strain of the hydrogel was recorded as the degree of deformation when the sample broke. According to the volume fraction changes after hydration and mechanical properties, the mesh size of the hydrogels could be determined by the following equation³⁶

$$\tau_s = \left[\frac{\nu_e}{V} \right] \frac{(\phi_2/\phi_0)^{2/3}}{RT(\alpha - \alpha^{-2})} \quad (2)$$

where τ_s stands for the stress at a particular strain, in units of Pa, α is the deformation ratio related to the stress determined as the ratio of the elastically deformed length to the initial length of hydrogel under compression, R is the universal gas constant, T is the absolute temperature, ϕ_2 represents the volume fraction of the fully swollen hydrogel, and ϕ_0 represents the volume fraction of hydrogel in the relaxed state. At low strain, the plot of τ_s vs $(\alpha - \alpha^{-2})$ is linear, and the cross-link density (ν_e/V) can be extracted from the slope (ν_e/V)(RT)(ϕ_2/ϕ_0) $^{-2/3}$.

The cross-link density can be converted to the mesh size by following equation

$$\xi = \left[\frac{\nu_e N_A}{V} \right]^{-1/3} \quad (3)$$

where ξ stands for the definite mesh size of the hydrogels and N_A represents Avogadro's number.

UV–Vis Absorption Measurement. The fully equilibrated hydrogel samples were punched into 8-mm-diameter disks. Then the samples were spread into the 24-well plates and scanned by light with a wavelength from 300 to 600 nm.¹¹

Catalytic Reduction of 4-NP. In a typical run for the reduction of 4-NP by NaBH_4 ,³³ aqueous 4-NP solution ($600 \mu\text{L}$, 10 mM) was mixed with freshly prepared ice-cold NaBH_4 solution ($800 \mu\text{L}$, 0.5 M), resulting in a deep-yellow solution. After being diluted with ultrapure water to 4 mL, as-prepared AgNP-embedded hydrogels were subsequently introduced into the mixture. At regular intervals (every 60 s), the reaction was monitored by recording the UV–vis absorption spectra ($\lambda_{\text{max}} = 400 \text{ nm}$ for 4-NP) of $100 \mu\text{L}$ of the reaction solution.

Protein Adsorption Tests. FITC-BSA was used in protein adsorption tests. The fully equilibrated hydrogel samples of 8 mm diameter were washed with PBS buffer five times before tests. Under the light proof condition, the hydrogel samples were placed into a 24-well plate and incubated with $200 \mu\text{L}$ of FITC-BSA (2.5 mg/mL) solutions for 30 min. Before the observation under the inverted fluorescence microscope, the samples were washed with water five times to remove the extra FITC-BSA.

Catalytic Reduction of 4-NP in BSA Solutions. Before the catalytic reaction, a certain amount of BSA (the final concentration varied from 0.02 to 0.1 M) was dissolved in the ice-cold aqueous

NaBH_4 solution, and then the catalytic reaction was carried out as described above.

Recyclability of the Hydrogels. After the completion of the catalytic reaction, the AgNP-embedded hydrogels were separated by filtration. The recovered hydrogels were washed three times with water, and the excess water was removed and reused in the borohydride reduction reaction of 4-NP. The following reaction processes were carried out under the same reaction condition. The procedure mentioned previously was repeated for 10 successive cycles.

FTIR, SEM, and TEM Tests. For FTIR tests, the fully equilibrated hydrogel samples were gently crushed and freeze-dried at $-45 \text{ }^\circ\text{C}$, 0.04 MPa for 24 h. Then, completely dry hydrogel powders were collected and the sample-KBr pellets were tested using a Nexus 670 FTIR spectrophotometer with a wavenumber resolution of 0.5. For SEM tests, the prepared hydrogel particles with a dimension of $\sim 0.5 \text{ mm}^3$ were freeze-dried. Then, samples were observed with an S-4800 instrument at an accelerating voltage of 5 kV. For TEM tests, the ground hydrogel powders were subsequently resuspended in ethanol (1 mg/mL). The as-prepared mixtures were dropped onto a copper grid precoated with amorphous carbon and dried.¹⁶ Then, samples were tested using a JEM-2100F electron microscope.

Data Analysis. All examination and quantitative results were obtained from at least three samples. Results are expressed as the means of at least three replicates \pm SD (standard deviation). The error bars denote the SD ($n \geq 3$).

RESULTS AND DISCUSSION

Characterization of AgNP-Embedded Hydrogels. We evaluated the equilibrium water content (EWC), mechanical properties, and mesh sizes of different hydrogels. As shown in Figure 1a, the EWC of AgNP-embedded hydrogels was similar

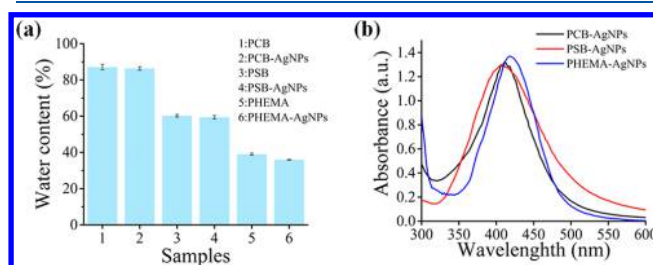


Figure 1. Properties of AgNP-embedded hydrogels. (a) Water content of PCB, PCB-AgNP, PSB, PSB-AgNP, PHEMA, and PHEMA-AgNP hydrogels. (b) UV–vis absorption spectra of PCB-AgNP, PSB-AgNP, and PHEMA-AgNP hydrogels with the same concentration of AgNO_3 (10 mM).

to that of the pure hydrogels (PCB, PSB, and PHEMA), indicating that the formation of AgNPs made no significant difference to the hydration properties. The EWC of PCB-AgNPs remained $>85\%$, which was much higher than that of PSB-AgNPs (53.42%) and PHEMA-AgNPs (35.93%). A higher water content could be more favorable to the facilitation of mass transfer in the hydrogel. In addition, the mechanical properties of different hydrogels are summarized in Table 1. The formation of AgNPs did not significantly alter the compressive modulus or break strain. Meanwhile, PCB-AgNPs displayed a higher compressive modulus and break strain than did PSB-AgNPs. Higher mechanical strength would be beneficial to maintaining the hydrogel integrity as a supporting matrix and enhancing the reusability in cyclic reactions. The mesh size of the hydrogels is also an important factor for mass transfer in the hydrogels. As shown in Table 1, the PCB hydrogel had the largest mesh size (3.57 nm),

Table 1. Physical Properties of AgNP-Embedded Hydrogels

sample	compressive modulus (MPa)	break strain (%)	mesh size (nm)	AgNPs concentration (mM)
PCB	0.157 ± 0.004	48.75 ± 1.53	3.57	
PCB-AgNPs	0.162 ± 0.004	47.20 ± 1.61		4.86
PSB	0.118 ± 0.008	34.72 ± 1.96	3.22	
PSB-AgNPs	0.120 ± 0.007	42.99 ± 1.45		5.26
PHEMA	0.262 ± 0.011		1.97	
PHEMA-AgNPs	0.280 ± 0.007			5.73

whereas the sizes of PSB and PHEMA hydrogels were 3.22 and 1.97 nm, respectively. The larger mesh size could endow the PCB hydrogel with more efficient mass transfer and thus might accelerate the catalytic rate.

SEM images in Figure 2 showed that both the PCB and PCB-AgNP hydrogels exhibited compact bulk structures since

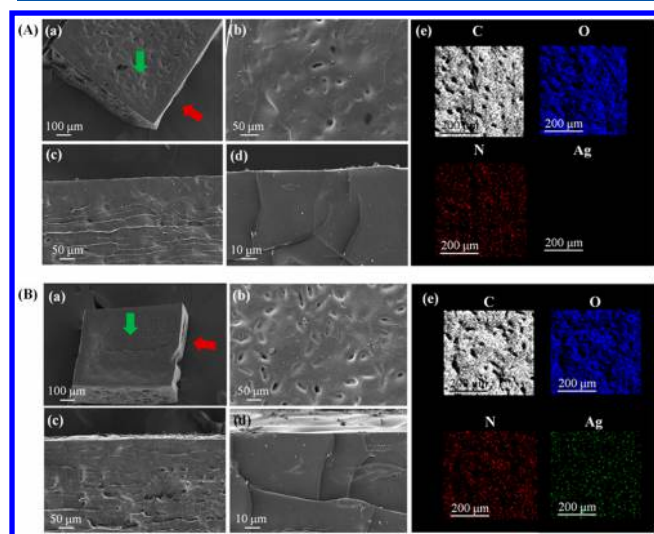


Figure 2. SEM images of (A) PCB and (B) PCB-AgNP hydrogels. (a) Three-dimensional structure of PCB and PCB-AgNP hydrogels. (b) Surface morphology of PCB and PCB-AgNP hydrogels (indicated by the green arrow in panel a). (c, d) Lateral morphology of PCB and PCB-AgNP hydrogels (indicated by the red arrow in panel a). (e) EDS signals of PCB and PCB-AgNP hydrogels mapping the C, O, N, and Ag elements at the surface (indicated by the green arrow in panel a).

the mesh size of the PCB hydrogel was on the nanometer scale. In addition, PCB-AgNPs and pure PCB hydrogels were similar in terms of morphology and topography (Figure 2A,B), indicating that the formation of AgNPs had no significant effect on hydrogel structures.

Characterization of in-Situ-Formed AgNPs. AgNP formation was characterized by the UV spectral method (Figure 1b). The resulting hydrogels showed an absorption peak at ~410 nm, indicating the formation of AgNPs in the hydrogels. The absorption peaks were similar to those of AgNPs formed in aqueous solutions, confirming that Ag was in the form of nanoparticles. Compared to 20 mM AgNO₃ samples (Figure S1a), all kinds 10 mM AgNO₃ samples showed absorption peaks at ~410 nm without the obvious red shift,³⁷ indicating a more effective formation of AgNPs, thus they were chosen for subsequent work (Figure 1b). Energy-dispersive spectroscopy (EDS) tests also confirmed the uniform Ag distribution in PCB-AgNP hydrogels (Figure 2B).

The size distribution and morphology of AgNPs were then characterized by TEM tests. The results (Figures 3 and Figure

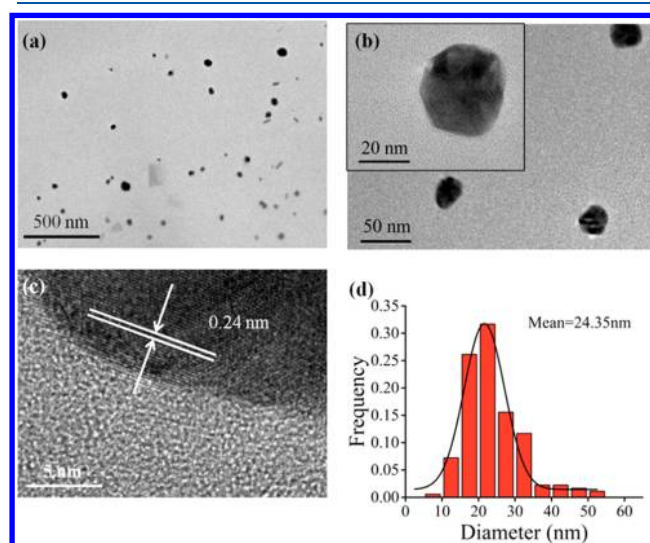


Figure 3. (a, b) TEM images of AgNPs (10 mM AgNO₃) formed inside the PCB hydrogel. (c) HRTEM image showing the lattice fringes of AgNPs. (d) Size distribution histogram of the AgNPs.

S2) showed that the monodisperse AgNPs were uniformly distributed with an average diameter of 24.35 nm in the hydrogels. Moreover, high-resolution transmission electron microscopy (HRTEM) was used to determine the crystalline structure of AgNPs. As shown in Figures 3c and S2c, the lattice fringes were visible with ~0.24 nm spacings, corresponding to the lattice spacings of Ag(111). In accordance with the red shift in the UV spectra, the AgNPs made from 20 mM AgNO₃ had an average diameter of 40.27 nm (Figure S2), which was almost twice the diameter of 10 mM AgNO₃.

FTIR spectroscopy was further employed to analyze the AgNP-embedded hydrogels (Figure 4). For PCB and PCB-AgNPs (Figure 4a), the peak at around 3273 cm⁻¹ corresponded to the stretching vibration of O–H. The band at 1655 cm⁻¹ was the characteristic peak of amide groups. The peaks at 1590 and 1377 cm⁻¹ were assigned to the asymmetric and symmetric stretching of –COOH, respectively. As shown in Figure 4b, the broad band at around 3445 cm⁻¹ could be assigned to the O–H stretching of –COOH in PSB and PSB-AgNP hydrogels. The characteristic peak of ester carbonyl was observed at 1729 cm⁻¹, and the peak at 1485 cm⁻¹ was associated with quaternary ammonium.^{38,39} Both PSB and PSB-AgNP hydrogels exhibited distinct adsorption bands at 1185 and 1041 cm⁻¹, corresponding to the S=O asymmetric and symmetric stretches, respectively.³⁵ In Figure 4c, the stretching vibrations at 3437 and 1727 cm⁻¹ presented the hydroxyl and carbonyl in PHEMA and PHEMA-AgNP hydrogels.³⁹ The FTIR spectra of PCB-AgNP, PSB-AgNP,

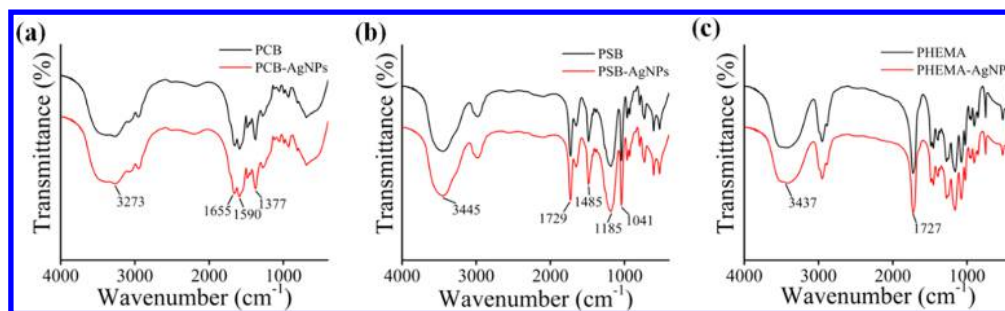


Figure 4. FTIR spectra of (a) PCB and PCB-AgNP hydrogels. (b) PSB and PSB-AgNP hydrogels. (c) PHEMA and PHEMA-AgNP hydrogels.

and PHEMA-AgNP hydrogels were almost identical to that of pure PCB, PSB, and PHEMA hydrogels, respectively. These results suggested that in-situ-formed AgNPs did not affect the properties of pristine hydrogels or form extra bonds with them.

Catalytic Activities of AgNP-Embedded Hydrogels.

The catalytic activity of AgNPs was then evaluated in the 4-NP reduction reaction (Figure 5a).⁴⁰ Although the reaction is a

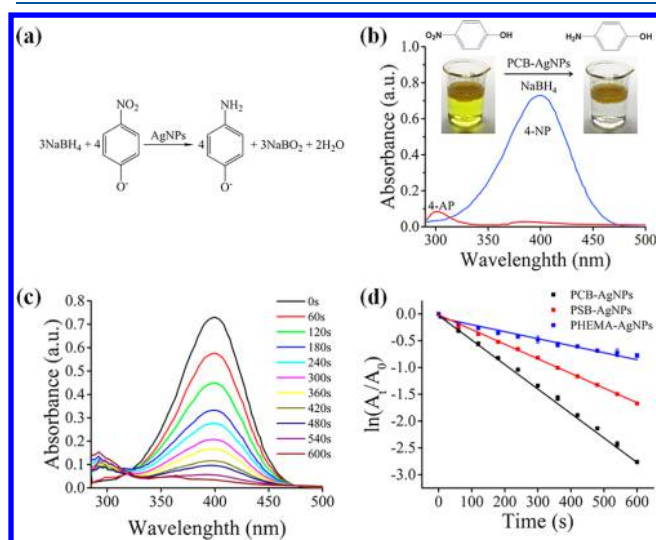


Figure 5. (a) Reduction of 4-NP to 4-AP catalyzed by AgNPs. (b) Changes in the UV-vis spectra during the reduction of 4-NP catalyzed by PCB-AgNPs (before the reduction, blue line; after the reduction, red line). (c) Time-dependent UV-vis spectra of the 4-NP reduction catalyzed by PCB-AgNPs. (d) $\ln(A_t/A_0)$ versus reaction time for the 4-NP reduction catalyzed by PCB-AgNPs, PSB-AgNPs, and PHEMA-AgNPs.

thermodynamically feasible process involving standard electrode potentials (E_0) of -0.76 V (4-NP/4-AP) and -1.33 V ($\text{H}_3\text{BO}_3/\text{BH}_4^-$) versus NHE, it is still kinetically restricted in the absence of catalysts (does not react for 2 days).¹¹ AgNPs could catalyze the reduction by relaying electrons from the donor (BH_4^-) to the acceptor (4-NP). As shown in Figure 5b, after adding PCB-AgNPs, the reaction proceeded rapidly and the solution faded to colorless within only 60 s. The reaction was quantitatively verified by UV-vis spectra with the increased absorbance of 4-AP at ~ 300 nm and the decreased absorbance of 4-NP at ~ 400 nm (Figure 5b,c).³⁵ Then, kinetic data were fitted with a pseudo-first-order model³³

$$\ln(C_t/C_0) = \ln(A_t/A_0) = k_{\text{app}}t \quad (4)$$

where C_0 and C_t represent the concentration of 4-NP at the initial time and at time t . In this experiment, the ratio of C_t to

C_0 could be directly given by the ratio of respective absorbance A_t/A_0 . (A is the absorbance at 400 nm.) k_{app} is the apparent first-order rate constant (s^{-1}).⁴¹ According to the apparent first-order rate equation (eq 4), when $\ln(A_t/A_0)$ is proportional to time t , the reaction rate corresponds to the slope of the curve, k_{app} .

To evaluate the influence of supporting hydrogels, PSB-AgNPs and PHEMA-AgNPs were also used to reduce 4-NP under the same conditions. All three kinds of AgNP-embedded hydrogels showed catalytic activity (Figure 5d) for 4-NP reduction. A linear relation between $\ln(A_t/A_0)$ and reaction time t was observed, which well matched the first-order reaction kinetics. As shown in Table 2, k_{app} values for the

Table 2. Catalytic Data for 4-NP Reduction by AgNP-Embedded Hydrogels

catalyst	catalyst used (mmol)	k_{app} (s^{-1})	k_{nor} ($\text{s}^{-1} \text{mmol}^{-1}$)
PCB-AgNPs	4.05×10^{-4}	4.30×10^{-3}	10.617
PSB-AgNPs	4.38×10^{-4}	2.73×10^{-3}	6.233
PHEMA-AgNPs	4.78×10^{-4}	1.31×10^{-3}	2.741

reactions using PCB-AgNPs, PSB-AgNPs, and PHEMA-AgNPs were calculated to be 4.30×10^{-3} , 2.73×10^{-3} , and $1.31 \times 10^{-3} \text{ s}^{-1}$, respectively. After normalization by the AgNP amount, the k_{nor} values of PCB-AgNPs, PSB-AgNPs, and PHEMA-AgNPs were 10.617, 6.233, and $2.741 \text{ s}^{-1} \text{mmol}^{-1}$, respectively. PCB-AgNPs displayed the best catalytic performance compared to the PSB-AgNPs or PHEMA-AgNPs. For PHEMA-AgNPs, the smallest mesh size (1.97 nm) might limit the mass transfer rate during the catalytic reaction. The mesh size of PCB-AgNPs and PSB-AgNPs was much larger (3.57 and 3.22 nm) than that of PHEMA-AgNPs, which would benefit the mass transfer. In addition, owing to the superhydrophilicity of the zwitterionic hydrogel, hydrosoluble 4-NP and 4-AP could more sufficiently contact AgNPs in the hydrogels, and the electron transfer from BH_4^- to 4-NP could be more rapid surrounded by a hydrophilic environment. Notably, a higher k_{app} was observed in the PCB-AgNPs group compared to PSB-AgNPs. This might be attributed to the strongest hydration, few self-associations, and the large mesh size of the PCB hydrogel. The catalytic data for 4-NP reduction using different nanocatalysts in previous reports are summarized in Table 3. The k_{nor} value of as-prepared PCB-AgNPs was $10.617 \text{ s}^{-1} \text{mmol}^{-1}$, indicating a much higher catalytic activity than for relevant reports in the table. PCB-AgNP hydrogels also had a smaller AgNP size and comparable recyclability in comparison to other representative reports of metal nanoparticle-hydrogel catalysts (Tables 3 and S3).

Table 3. Reports on the 4-NP Reduction by Various Metal Nanoparticle Catalysts

catalyst	catalyst used (mmol)	k_{app} (s^{-1})	k_{nor} ($s^{-1} \text{ mmol}^{-1}$)	water content (%)	particle size (nm)	recyclability/cycle number	refs
PCB-AgNPs	4.05×10^{-4} (Ag)	4.30×10^{-3}	10.617	87.11	20–30	96%/10	this work
p(AMPS)-Ni	1.01×10^{-1} (Ni)	9.38×10^{-4}	0.009	22.62	50–100	75%/5	42
p(AMPS)-Co	1.00×10^{-1} (Co)	2.00×10^{-3}	0.020	19.27	50–100	78%/5	43
Ag/nanosilica	6.7×10^{-4} (Ag)	7.57×10^{-4}	1.130		21	92%/3	10
Ag/C spheres	5.11×10^{-3} (Ag)	1.69×10^{-3}	0.331		800		44
Ag/nanodendrites	1.85×10^{-2} (Ag)	5.63×10^{-3}	0.304		~35		9
FAC-Au-1.5	1.15×10^{-2} (Au)	11.0×10^{-3}	0.956		~100	~20%/7	33

Catalytic Activities of the AgNP-Embedded Hydrogels in BSA Solutions. AgNPs can catalyze the reduction by relaying electrons between the reactant and the reductant, thus the surface contact between AgNPs and 4-NP is a prerequisite for 4-NP reduction. However, some charged macromolecules such as proteins are liable to adsorb to the nanocatalysts via electrostatic interactions, compromising the effective contact area and even causing irreversible structural changes in the nanocatalysts. In this work, FITC-BSA was used as a model protein to evaluate the antibiofouling ability of PCB-AgNPs. In the static protein adsorption tests, fluorescence microscopy images proved that no significant FITC-BSA attachment was observed on the surfaces of the PCB, PSB, PCB-AgNP, and PSB-AgNP hydrogels (Figure 6), which was consistent with previous studies.^{15–17,34} In contrast, both PHEMA and PHEMA-AgNP hydrogels showed a considerable amount of FITC-BSA adsorption (Figure 6).

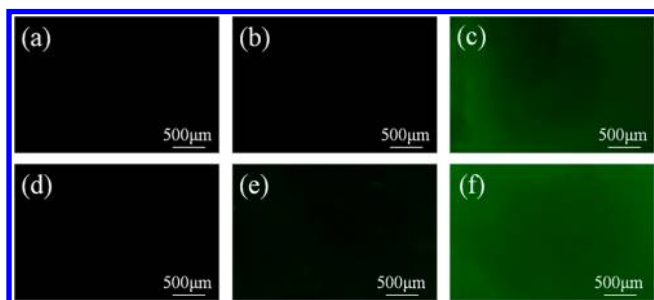


Figure 6. Fluorescence microscopy images of the FITC-BSA adsorption of (a) PCB, (b) PSB, (c) PHEMA, (d) PCB-AgNP, (e) PSB-AgNP, and (f) PHEMA-AgNP hydrogels.

In the dynamic catalytic tests, BSA solutions with a gradient concentrations from 0.02 to 0.1 M were used. As shown in Figure 7, a good linear correlation was found between $\ln(A_t/A_0)$ and reaction time t in 0.1 M BSA solutions. (The results of 0.02 and 0.05 M BSA solutions are shown in Figure S3.) PCB-AgNPs in 0.1 M BSA solutions exhibited almost the same k_{app} as in BSA-free solutions, whereas k_{app} of PHEMA-AgNPs decreased by 62% (Figure 7). The results demonstrated that the catalytic activity of PCB-AgNPs was not compromised in a biofouling environment. The poor performance of PHEMA-AgNPs in BSA solutions might be attributed to the limited antifouling ability of the PHEMA hydrogel.⁴⁵

Recyclability and Storage Stability. The recyclability of catalysts is a considerable factor in practical applications. In this work, the recyclability of PCB-AgNPs was investigated by the conversion of 4-NP for 30 min. The conversion of 4-NP to 4-AP was calculated with the following equation

$$\text{conversion} = (1 - A_t/A_0) \times 100\% \quad (5)$$

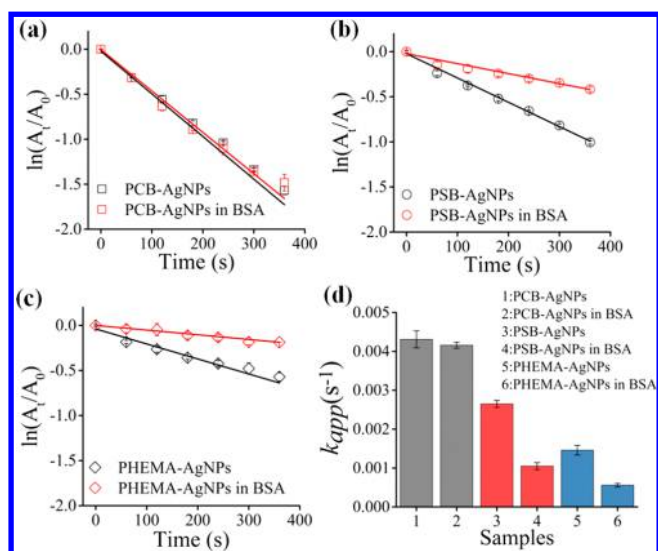


Figure 7. $\ln(A_t/A_0)$ versus reaction time for the reduction of 4-NP using (a) PCB-AgNPs, (b) PSB-AgNPs, and (c) PHEMA-AgNPs in BSA-free (black line) and BSA solutions (red line). (d) k_{app} of reactions catalyzed in BSA-free and BSA solutions.

A_t represents the UV absorbance at 400 nm, which is proportional to the concentration of produced 4-NP. A_0 is the initial UV absorbance at ~400 nm after the addition of NaBH_4 .

As shown in Figures 8a and S4, after 10 cycles, PCB-AgNPs could still maintain a >95% conversion efficiency, presenting a

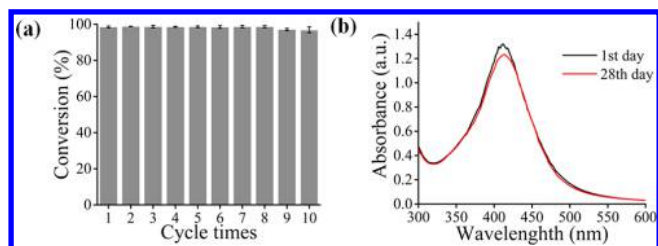


Figure 8. (a) Conversion efficiency of 4-NP with PCB-AgNPs for 30 min and 10 successive cycles; (b) UV/vis absorption spectrum of PCB-AgNPs on the first day and 28th day.

recyclability comparable to that in previous reports (Tables 3 and S3).^{42–44,46} Furthermore, from the UV–vis spectra of the reaction solutions, the concentration change of AgNPs was negligible (data not shown), indicating that there was no obvious leakage of AgNPs. Moreover, after storage at 4 °C for 28 days, the UV–vis spectrum of PCB-AgNPs was similar to that of the first day (Figure 8b), indicating no significant

aggregation or leakage of AgNPs during the whole storage period.

CONCLUSIONS

In this work, a facile photochemical method for the in situ AgNP synthesis and encapsulation in zwitterionic hydrogels has been developed. AgNPs with an average size of ~ 25 nm were uniformly distributed inside the PCB hydrogel without aggregation. PCB-AgNPs had the best catalytic activity ($k_{\text{nor}} = 10.617 \text{ s}^{-1} \text{ mmol}^{-1}$) for the reduction of 4-NP to 4-AP compared to PSB-AgNPs and PHEMA-AgNPs, owing to the strong hydrophilic property and larger mesh size required to facilitate the mass transfer. Moreover, the outstanding antibiofouling property enabled PCB-AgNPs to maintain their catalytic ability in environments containing protein. Excellent catalytic activity, antibiofouling ability, and recyclability render the PCB-AgNPs a promising catalyst for the degradation of hazardous nitroaromatic compounds.

ASSOCIATED CONTENT

Supporting Information

The Supporting Information is available free of charge on the ACS Publications website at DOI: [10.1021/acs.langmuir.8b02918](https://doi.org/10.1021/acs.langmuir.8b02918).

Characterization of PCB-AgNPs prepared with varied concentrations of AgNO_3 solutions; catalytic efficiency of PCB-AgNPs prepared with varied concentrations of AgNO_3 solutions; catalytic efficiency of PCB-AgNPs, PSB-AgNPs, and PHEMA-AgNPs in different concentrations of BSA solutions; comparison of AgNP catalysts for 4-NP reduction with relevant reports; and conversion efficiency of PCB-AgNPs in 10 successive cycles (PDF)

AUTHOR INFORMATION

Corresponding Author

*E-mail: lei_zhang@tju.edu.cn.

ORCID

Lei Zhang: [0000-0003-3638-6219](https://orcid.org/0000-0003-3638-6219)

Author Contributions

[†]These authors contributed equally to this work

Notes

The authors declare no competing financial interest.

ACKNOWLEDGMENTS

This work was supported by funds from the National Natural Science Funds for Innovation Research Groups (21621004), the Qingdao National Laboratory for Marine Science and Technology (QNL2016ORP0407), Tianjin Natural Science Foundation (18JCYB- JC29500), and the National Natural Science Funds for Excellent Young Scholars (21422605).

REFERENCES

- (1) Li, T.; Vongehr, S.; Tang, S.; Dai, Y.; Huang, X.; Meng, X. Scalable Synthesis of Ag Networks with Optimized Sub-monolayer Au-Pd Nanoparticle Covering for Highly Enhanced SERS Detection and Catalysis. *Sci. Rep.* **2016**, *6*, 37092.
- (2) Castonguay, A.; Kakkar, A. K. Dendrimer templated construction of silver nanoparticles. *Adv. Colloid Interface Sci.* **2010**, *160* (1), 76–87.
- (3) Zhang, Y.; Yuan, X.; Wang, Y.; Chen, Y. One-pot photochemical synthesis of graphene composites uniformly deposited with silver

nanoparticles and their high catalytic activity towards the reduction of 2-nitroaniline. *J. Mater. Chem.* **2012**, *22* (15), 7245–7251.

- (4) Zhang, P.; Shao, C.; Zhang, Z.; Zhang, M.; Mu, J.; Guo, Z.; Liu, Y. In situ assembly of well-dispersed Ag nanoparticles (AgNPs) on electrospun carbon nanofibers (CNFs) for catalytic reduction of 4-nitrophenol. *Nanoscale* **2011**, *3* (8), 3357–3363.

- (5) Jiang, D.; Xie, J.; Chen, M.; Li, D.; Zhu, J.; Qin, H. Facile route to silver submicron-sized particles and their catalytic activity towards 4-nitrophenol reduction. *J. Alloys Compd.* **2011**, *509* (5), 1975–1979.

- (6) Zhang, W.; Sun, Y.; Zhang, L. In Situ Synthesis of Monodisperse Silver Nanoparticles on Sulfhydryl-Functionalized Poly(glycidyl methacrylate) Microspheres for Catalytic Reduction of 4-Nitrophenol. *Ind. Eng. Chem. Res.* **2015**, *54*, 6480.

- (7) Rao, J. R.; Chandrababu, N. K.; Muralidharan, C.; Nair, B. U.; Rao, P. G.; Ramasami, T. Recouping the wastewater: a way forward for cleaner leather processing. *J. Cleaner Prod.* **2003**, *11* (5), 591–599.

- (8) Geng, Q.; Du, J. Reduction of 4-nitrophenol catalyzed by silver nanoparticles supported on polymer micelles and vesicles. *RSC Adv.* **2014**, *4* (32), 16425–16428.

- (9) Zhang, W.; Tan, F.; Wang, W.; Qiu, X.; Qiao, X.; Chen, J. Facile, template-free synthesis of silver nanodendrites with high catalytic activity for the reduction of p-nitrophenol. *J. Hazard. Mater.* **2012**, *217–218* (3), 36–42.

- (10) Das, S. K.; Khan, M. M. R.; Guha, A. K.; Naskar, N. Bio-inspired fabrication of silver nanoparticles on nanostructured silica: characterization and application as a highly efficient hydrogenation catalyst. *Green Chem.* **2013**, *15* (9), 2548–2557.

- (11) Saha, S.; Pal, A.; Kundu, S.; Basu, S.; Pal, T. Photochemical Green Synthesis of Calcium-Alginate-Stabilized Ag and Au Nanoparticles and Their Catalytic Application to 4-Nitrophenol Reduction. *Langmuir* **2010**, *26* (4), 2885.

- (12) Sangeetha, N. M.; Maitra, U. Supramolecular gels: Functions and uses. *Chem. Soc. Rev.* **2005**, *34* (10), 821–836.

- (13) Lowe, A. B.; McCormick, C. L. Synthesis and solution properties of zwitterionic polymers. *Chem. Rev.* **2002**, *102* (11), 4177–4189.

- (14) Zhang, Q.; Zhang, S.; Dai, L.; Chen, X. Novel zwitterionic poly(arylene ether sulfone)s as antifouling membrane material. *J. Membr. Sci.* **2010**, *349* (1), 217–224.

- (15) Zhang, Z.; Zhang, M.; Chen, S.; Horbett, T. A.; Ratner, B. D.; Jiang, S. Blood compatibility of surfaces with superlow protein adsorption. *Biomaterials* **2008**, *29* (32), 4285–4291.

- (16) Zhu, Y.; Zhang, J.; Song, J.; Yang, J.; Xu, T.; Pan, C.; Zhang, L. One-step synthesis of an antibacterial and pro-healing wound dressing that can treat wound infections. *J. Mater. Chem. B* **2017**, *5* (43), 8451–8458.

- (17) Cai, N.; Li, Q.; Zhang, J.; Xu, T.; Zhao, W.; Yang, J.; Zhang, L. Antifouling zwitterionic hydrogel coating improves hemocompatibility of activated carbon hemoabsorbent. *J. Colloid Interface Sci.* **2017**, *503*, 168–177.

- (18) Tagawa, T.; Takahashi, H.; Sekiguchi, Y.; Ohashi, A.; Harada, H. Pilot-plant study on anaerobic treatment of a lipid- and protein-rich food industrial wastewater by a thermophilic multi-staged UASB reactor. *Water Sci. Technol.* **2002**, *45* (10), 225–230.

- (19) Carrier, M.; Besson, M.; Guillard, C.; Gonze, E. Treatment of agricultural wastewater containing herbicides by Advanced Oxidation Processes. *J. Biol. Chem.* **2005**, *265* (22), 12782–5.

- (20) Raunkjær, K.; Hvitved-Jacobsen, T.; Nielsen, P. H. Measurement of pools of protein, carbohydrate and lipid in domestic wastewater. *Water Res.* **1994**, *28* (2), 251–262.

- (21) Sun, S. P.; Lemley, A. T. p-Nitrophenol degradation by a heterogeneous Fenton-like reaction on nano-magnetite: Process optimization, kinetics, and degradation pathways. *J. Mol. Catal. A: Chem.* **2011**, *349* (1), 71–79.

- (22) Chiou, J. R.; Lai, B. H.; Hsu, K. C.; Chen, D. H. One-pot green synthesis of silver/iron oxide composite nanoparticles for 4-nitrophenol reduction. *J. Hazard. Mater.* **2013**, *248–249* (1), 394–400.

- (23) Feng, J.; Su, L.; Ma, Y.; Ren, C.; Guo, Q.; Chen, X. CuFe₂O₄ magnetic nanoparticles: A simple and efficient catalyst for the reduction of nitrophenol. *Chem. Eng. J.* **2013**, *221* (4), 16–24.
- (24) Torresmartínez, C. L.; Kho, R.; Mian, O. I.; Mehra, R. K. Efficient Photocatalytic Degradation of Environmental Pollutants with Mass-Produced ZnS Nanocrystals. *J. Colloid Interface Sci.* **2001**, *240* (2), 525–532.
- (25) Oturan, M. A.; et al. Complete Destruction of p-Nitrophenol in Aqueous Medium by Electro-Fenton Method. *Environ. Sci. Technol.* **2000**, *34* (16), 3474–3479.
- (26) Borrás, C.; Laredo, T.; Scharifker, B. R. Competitive electrochemical oxidation of -chlorophenol and -nitrophenol on Bi-doped PbO. *Electrochim. Acta* **2003**, *48* (19), 2775–2780.
- (27) Swathi, T.; Buvanewari, G. Application of NiCo₂O₄ as a catalyst in the conversion of p -nitrophenol to p -aminophenol. *Mater. Lett.* **2008**, *62* (23), 3900–3902.
- (28) Chi, Y.; et al. Synthesis of Fe₃O₄@SiO₂-Ag magnetic nanocomposite based on small-sized and highly dispersed silver nanoparticles for catalytic reduction of 4-nitrophenol. *J. Colloid Interface Sci.* **2012**, *383* (1), 96–102.
- (29) Liang, M.; Su, R.; Huang, R.; Qi, W.; Yu, Y.; Wang, L.; He, Z. Facile in situ synthesis of silver nanoparticles on procyanidin-grafted eggshell membrane and their catalytic properties. *ACS Appl. Mater. Interfaces* **2014**, *6* (7), 4638–49.
- (30) Liang, Y.; Chen, Z.; Yao, W.; Wang, P.; Yu, S.; Wang, X. Decorating of Ag and CuO on Cu Nanoparticles for Enhanced High Catalytic Activity to the Degradation of Organic Pollutants. *Langmuir* **2017**, *33* (31), 7606.
- (31) Bao, Z.; Yue, Y.; Leng, C.; Li, L.; Zhao, K.; Sun, Z. One-Pot Synthesis of Noble Metal/Zinc Oxide Composites with Controllable Morphology and High Catalytic Performance. *ACS Appl. Mater. Interfaces* **2017**, *9* (19), 16417.
- (32) Qu, J. C.; Ren, C. L.; Dong, Y. L.; Chang, Y. P.; Zhou, M.; Chen, X. G. Facile synthesis of multifunctional graphene oxide/AgNPs-Fe₃O₄ nanocomposite: A highly integrated catalysts. *Chem. Eng. J.* **2012**, *211–212* (47), 412–420.
- (33) Rashid, M. H.; Mandal, T. K. Templateless Synthesis of Polygonal Gold Nanoparticles: An Unsupported and Reusable Catalyst with Superior Activity. *Adv. Funct. Mater.* **2008**, *18* (15), 2261–2271.
- (34) Carr, L.; Cheng, G.; Xue, H.; Jiang, S. Engineering the polymer backbone to strengthen nonfouling sulfobetaine hydrogels. *Langmuir* **2010**, *26* (18), 14793–14798.
- (35) Dauthal, P.; Mukhopadhyay, M. Prunus domestica Fruit Extract-Mediated Synthesis of Gold Nanoparticles and Its Catalytic Activity for 4-Nitrophenol Reduction. *Ind. Eng. Chem. Res.* **2012**, *51* (40), 13014–13020.
- (36) Kamath, K. R.; Park, K. Biodegradable Hydrogels for Drug Delivery. *Adv. Drug Delivery Rev.* **1993**, *11* (1–2), 59–84.
- (37) Paramelle, D.; Sadovoy, A.; Gorelik, S.; Free, P.; Hopley, J.; Fernig, D. G. A rapid method to estimate the concentration of citrate capped silver nanoparticles from UV-visible light spectra. *Analyst* **2014**, *139* (19), 4855–61.
- (38) Li, J. H.; Li, M. Z.; Miao, J.; Wang, J. B.; Shao, X. S.; Zhang, Q. Q. Improved surface property of PVDF membrane with amphiphilic zwitterionic copolymer as membrane additive. *Appl. Surf. Sci.* **2012**, *258* (17), 6398–6405.
- (39) Lalani, R.; Liu, L. Synthesis, characterization, and electrospinning of zwitterionic poly(sulfobetaine methacrylate). *Polymer* **2011**, *52* (23), 5344–5354.
- (40) Lu, Y.; et al. Thermosensitive core-shell particles as carriers for ag nanoparticles: modulating the catalytic activity by a phase transition in networks. *Angew. Chem., Int. Ed.* **2006**, *45* (5), 813–816.
- (41) Lara, L. S.; Zottis, A.; Elias, W.; Faggion, D.; Madurodecampos, C.; Acuna, J.; Domingos, J. The catalytic evaluation of in situ grown Pd nanoparticles on the surface of Fe₃O₄@dextran particles in the p-nitrophenol reduction reaction. *RSC Adv.* **2015**, *5* (11), 8289–8296.
- (42) Sahiner, N.; Ozay, H.; Ozay, O.; Aktas, N. New catalytic route: Hydrogels as templates and reactors for in situ Ni nanoparticle synthesis and usage in the reduction of 2- and 4-nitrophenols. *Appl. Catal., A* **2010**, *385* (1), 201–207.
- (43) Sahiner, N.; Ozay, H.; Ozay, O.; Aktas, N. A soft hydrogel reactor for cobalt nanoparticle preparation and use in the reduction of nitrophenols. *Appl. Catal., B* **2010**, *101* (1), 137–143.
- (44) Tang, S.; Vongehr, S.; Meng, X. Carbon Spheres with Controllable Silver Nanoparticle Doping. *J. Phys. Chem. C* **2010**, *114* (2), 977–982.
- (45) Carr, L. R.; Xue, H.; Jiang, S. Functionalizable and nonfouling zwitterionic carboxybetaine hydrogels with a carboxybetaine dimethacrylate crosslinker. *Biomaterials* **2011**, *32* (4), 961–968.
- (46) Dolatkhan, A.; Jani, P.; Wilson, L. D. Redox-Responsive Polymer Template as an Advanced Multifunctional Catalyst Support for Silver Nanoparticles. *Langmuir* **2018**, *34* (36), 10560–10568.